BauSIM 2024 in Wien
23. September – 26. September

# Enhancing Efficiency and Feasibility of Large-Scale Thermal Energy Storage in District Heating

Abdulrahman Dahash, Fabrizia Giordano, Ahmed Serageldin
*AIT Austrian Institute of Technology GmbH, Center for Energy, Giefinggasse 2, 1210 Vienna, Austria, E-Mail: abdulrahman.dahash@ait.ac.at*

## Abstract

A key lever to overcome the challenges in the buildings sector related to today's extensive utilization of fossil fuels is the introduction of renewables-based district energy systems. Herein, large-scale seasonal thermal energy storage (STES) systems found its place favorably in these systems. Yet, STES systems require a thorough planning to avoid the high investment cost. Consequently, numerical models gain importance as an alternative to real-life experiments. This work investigates the role of insulation distribution within storage envelope on performance and capital cost. It further conducts a techno-economic assessment of large-scale, underground, seasonal thermal energy storage to reveal the role of insulation.

## Introduction

The building stock accounts for approximately 40% of the total energy consumption in European Union (EU), half of which goes for heating and cooling demands that are predominantly reliant on conventional fossil fuels (e.g. natural gas) (Maduta et al., 2022). The combustion of these fuels significantly contributes to $CO_2$ emissions, contradicting emission reduction goals (D'Agostino et al., 2024) by 2050. Consequently, decarbonizing the building sector becomes crucial, aligning with the integration of renewable energy sources (RESs). District heating (DH) emerges as an efficient solution to fulfill heating demand (K. Johansen and S. Werner, 2022). Despite its effectiveness, many DH systems still rely on natural gas, posing challenges impaired EU (Jodeiri et al., 2022).

The substitution of fossil fuels with RESs presents a viable solution, although it introduces challenges, including intermittent availability and storage difficulties. Thermal energy storage (TES) systems address these challenges, offering both short and long-term storage capabilities, thereby enhancing energy system robustness and facilitating sector coupling. Consequently, the integration of TES systems becomes pivotal for efficient energy management and increasing the share of RES.

Large-scale seasonal thermal energy storage (STES) has recently gained an increasing awareness for its capacity to mitigate mismatches between heat supply and demand (Dahash et al., 2020). Among STES methods, tank TES (TTES) and pit TES (PTES) stand out for their ability to achieve higher storage temperatures, primarily using water as a storage medium. This characteristic enables them to offer higher charging/discharging rates, reducing response time and reliance on backup heaters compared to other STES methods such as aquifer TES (ATES), and borehole TES (BTES) (Yuan et al., 2021). While BTES and ATES manage to store thermal energy at relatively lower temperatures and, hence, lower capital costs compared, TTES and PTES have higher capital costs.

Therefore, this study focuses primarily on TTES systems due to their relevance in addressing planning challenges in underground TES systems. By exploring these challenges, the work aims to contribute to the comprehension and optimization of TTES implementations in the context of energy system transitions.

## Literature review

Previous studies highlighted the complex nature of designing, planning and constructing large-scale TES systems. For instance, (Dahash et al., 2021) highlighted the interaction of various variables e.g. location, size, TES geometry, and hydrogeological conditions in the planning of STES systems. They concluded that planning such technologies necessitates a holistic approach, recognizing that individual variables can exert significant influence on the overall planning process (see Figure 1). Consequently, simulation-driven planning has emerged as a valuable strategy to assess the impact of different boundary conditions on STES planning. Thus,

calibrated numerical TES models serve as essential tools in such investigations.

Using numerical simulations, (Tosatto et al., 2022) investigated the role of STES type and volume in two types of district heating (DH) systems. The study revealed that increasing the STES volume results in a notable reduction in specific heat losses. Additionally, it emphasized the importance of insulation in enhancing STES performance, particularly a significant performance improvement in PTES systems with insulation. The study also provided estimates of the capital costs associated with implementing TTES and PTES across a volume range of 100,000 $m^3$ to 2,000,000 $m^3$. Yet, the investigation considered two cases for TES insulation: fully insulated or non-insulated (only top-insulated).

(Huang et al., 2020) conducted a technical analysis (e.g., solar fraction, TES performance) to reveal the impact of TES insulation levels on system operation considering five configurations ranging from full insulation to no insulation. While the work demonstrated an increase in TES capacity with upper-half insulation, it did not include a cost-to-benefit analysis of insulation installation.

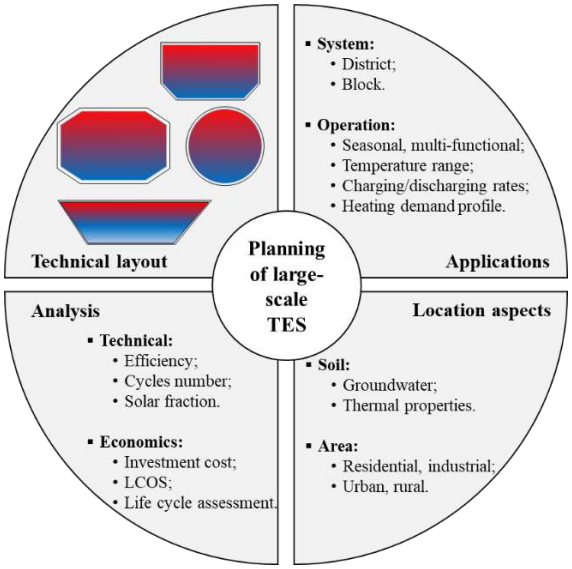


Figure 1: Several influencing parameters on the planning of underground TES and its economic feasibility (reproduced from (Dahash et al., 2021)).

### Contribution of this work

This work explores the role of insulation distribution and installation within the storage envelope on the technical viability and economic feasibility of large-scale, underground, seasonal thermal energy storage. The work briefly reports the development of the numerical model used for the investigation. Next, the work presents the boundary conditions and the application case. Then, the study lists down the key performance indicators used in the techno-economic assessment for such storage systems. Yet, the work is limited to consideration of tank thermal energy storage with a total volume of 100,000 $m^3$ and a height of 50 m in the subsurface. Besides, the study presumes investigations under favorable hydro-geological conditions (i.e. no groundwater existence or flowing).

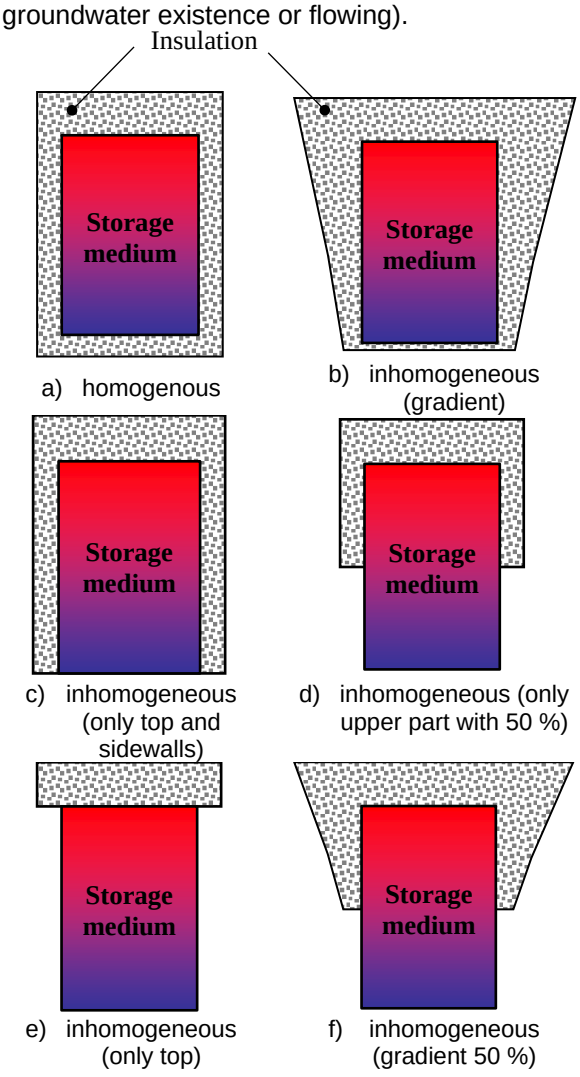


Figure 2: Homogenous and inhomogeneous insulation distribution for large-scale STES systems.

## Methodology

### Numerical modeling

To properly address the multi-physical aspects (i.e. conductive and convective heat transfer, and flow dynamics) in planning of large-scale STES, it is necessary to develop a numerical model with versatile capabilities such as the representation of different STES geometries, various STES envelopes and others (Dahash et al., 2021). Therefore, this work briefly reports the development of such a numerical model. The

developed model simulates a stratified TES, whereby the fluid domain can be discretized into (*n*) vertical nodes each with uniform temperature ($T_i$) and equal volume. Further information on the model development, calibration, validation and use can be found in (Dahash et al., 2021), (Tosatto et al., 2022) and (Dahash et al., 2020). Figure 3 elaborates a 2-D sketch for a buried TTES with a layer of aquifer zone (i.e. groundwater flow).

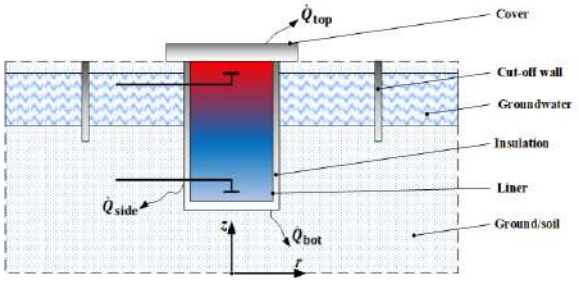


Figure 3: 2-D representation of a buried TES with: 1) cover, 2) cut-off wall, 3) groundwater, 4) insulation, 5) liner and 6) Ground domain.

The model obeys mass conservation and energy balance and, therefore, the time-dependent temperature distribution for each TES segment (i) can be described by the following expression:

$$\frac{\partial T_i(t)}{\partial t} = -\left(\frac{\dot{V}_w}{A_i}\right)\cdot\frac{\partial T_i}{\partial z_i} + \alpha\cdot\frac{\partial 2T_i}{\partial {z_i}^2} - \frac{\dot{q}_{loss,i}}{\rho A_i c_p} \quad (1)$$

Where $\rho$, $c_p$ and α represent the set of thermo-physical properties for the storage medium (i.e. water) and they are: the density, specific heat capacity and thermal diffusivity, respectively. The injected/extracted flowrate of each segment is denoted as ($\dot{V}_w$), whilst $A_i$ denotes the cross-section area of the corresponding segment (i). Each TES segment has an interface to the surrounding soil and, accordingly, any slight temperature difference between the TES fluid segment and the neighboring soil node triggers a heat transfer rate that is often accounted as heat losses form the TES. Thus:

$$\dot{q}_{loss,i} = U_{side}\cdot P_i\cdot(T_i(t) - T_{g,i}(t)) \quad (2)$$

Furthermore, it is noteworthy to highlight that the TES diffusers are assumed to be ideal due to the large TES volumes and, accordingly, low flowrates. Yet, the diffusers should be properly designed to ensure higher quality of stratification. Thus, CFD simulations are essential for this sort of investigations.

$$\rho_g c_{p,g}\frac{dT_g}{dt} = \lambda_g\left[\frac{\partial^2 T_g}{\partial z^2} + \frac{1}{r}\frac{\partial}{\partial r}\left(r\frac{\partial T_g}{\partial r}\right)\right] \quad (3)$$

Where $\rho_g$, $c_{p,g}$ and $\lambda_g$ define the density, specific heat capacity and thermal conductivity of the ground (i.e. subsurface soil). It is important to highlight that the work assumes the subsurface as a homogenous soil with same thermos-physical properties along depth of the subsurface. Moreover, the presence of groundwater is an important factor that needs to be considered in the planning of underground, large-scale TES. Yet, this work assumes favorable geological conditions in which no groundwater is present.

## Boundary conditions and assumptions

This work assumes seasonal operation of TTES whereby the charging phase starts early May and stops end of July with a constant injection temperature of 90°C. This phase is followed by a storage phase that starts early August and lasts 3 months. Once the heat is needed by beginning of November, TTES starts the discharging phase and the injection temperature into the TTES is 60°C. As TTES has no more useful energy for the DH needs, it operates in an idle phase. The injection volumetric flowrate is 0,01286 m³/s during both dynamic phases (i.e. charging and discharging). The ambient temperature is expressed as follows:

$$T_{amb} = 10 + sin\left(\frac{2\pi t}{365}\right) \quad (4)$$

Moreover, Table 1 reports the thermo-physical properties of the different domains (i.e. TES water, TES envelope, soil and groundwater) considered in this work.

Table 1: Thermo-physical properties of the materials and heat transfer coefficients (HTC) of the different components in TES and solid ground.

| Parameter | Value |
|---|---|
| Water thermal conductivity, $\lambda_w$ | 0.6 W/(m.K) |
| Water density, $\rho$ | 1000 kg/m³ |
| Water specific heat capacity, $c_p$ | 4200 J/(kg.K) |
| Overall HTC of the cover, $U_{top}$ | 0.15 W/(m².K) |
| Overall HTC of the sidewalls, $U_{side}$ | No insulation, 90 W/(m².K) |
| Overall HTC of the bottom, $U_{side}$ | No insulation, 90 W/(m².K) |
| Ground thermal conductivity, $\lambda_g$ | 1.5 W/(m.K) |
| Ground volumetric heat capacity, $c_{p,g}$ | MJ/(m³.K) |
| Ground density, $\rho_g$ | 1000 kg/m³ |

## Key performance indicators

In this work, three key performance indicators (KPIs) are used in order to estimate the technical performance of the considered TES system. These KPIs are energy efficiency and energy capacity efficiency used to evaluate the quantity of energy for the TES, while exergy efficiency arises as a promising tool for the optimization of TES design.

For the techno-economic analysis, the levelized cost of stored heat (LCOS) emerges as a key measure as it measures the average net present cost of stored heat across the lifecycle of the TES system under consideration. This indicator only accounts for the annualized investment cost (CAPEX) and the operation and maintenance cost (OPEX) that is 10 % of the CAPEX. LCOS does not account for additional cost for the TES decommissioning after the planned service lifetime. In this context, the service lifetime and the interest rate are 50 years and 3 %, respectively. Furthermore, the denominator ($\sum_{i=0}^{t} Q_{\mathrm{dis}}(t) \cdot \mathrm{d}t$) expresses the total amount of discharged heat for the examined year. Table 2 summarizes a list of KPIs used in this work and briefly reports the description of each metric considered. The reader is referred to (Dahash et al., 2021) if further information on the key performance indicators is needed.

Moreover, Table 3 reports a rough estimate of costs for several items in the construction of STES based on experience gained through previous projects and literature. Yet, these costs can be used to elaborate trends, but are still subject to high uncertainty. Yet, it is noteworthy to mention that these estimations represent the current state-of-the-art of the presented geotechnical solutions and not the technological improvement.

Table 2: List of the key performance indicators used in the techno-economic analysis framework adopted in this work (Dahash et al., 2021).

| KPI | Equation |
|---|---|
| Energy efficiency | $\eta_{\mathrm{I}} = \frac{Q_{\mathrm{dis}}}{Q_{\mathrm{ch}}}$ |
| Energy capacity efficiency | $\eta_{\mathrm{II}} = 1 - \frac{Q_{\mathrm{loss}}}{Q_{\mathrm{TES}}}$ |
| Exergy efficiency | $\psi = \frac{EX_{\mathrm{dis}}}{EX_{\mathrm{ch}}}$ |
| Levelized cost of stored heat (LCOS) | $\mathrm{LCOS} = \frac{(C_{\mathrm{inv}} \cdot ANF) + C_{\mathrm{O\&M}}}{\sum_{i=0}^{\tau} Q_{\mathrm{dis}}(t) \cdot \mathrm{d}t}$ |

Table 3: Breakdown of the specific costs for the construction of seasonal TES (Dahash et al., 2021).

| Contribution | Specific Costs | Remark |
|---|---|---|
| **Excavation** | 20 €/m³ | Partly wet excavation |
| **Diaphragm wall** | 550 €/m² | 50 m deep |
| **Sidewall** | 375 €/m³<br>100 €/m² | Insulation cost<br>Insulation installation |
| **Bottom** | 100 €/m³ | Insulation cost and installation (pressure resistant) |
| **Liner** | 150 €/m² | VA, Stainless steel |
| **Cover** | 200 €/m² | Floating cover (53 cm ins.) |
| **Plant construction** | 40,000 € | Independent TES construction |
| **Site facilities** | 50,000 € | Fixed |

## Results and discussion – Impact of insulation

The following section compares the different variants for the insulation distribution over the TES geometry. Herein, the common characteristics are: a fully buried tank with a total height of 50 m and a volume of 100,000 m$^3$. All insulation variants consider a top insulation thickness of 53 cm in order to produce $U_{\mathrm{top}}$ = 0.1 W/(m$^2$.K). Besides, the insulation material has a thermal conductivity of $\lambda_{\mathrm{ins}}$ = 0.08 W/(m.K). Moreover, Table 4 reports the different options for the insulation distribution that are considered in this investigation. Both configurations C and E feature insulation covering the upper 50% of the TES volume, while the remaining sidewalls remain uninsulated. Similarly, configurations B, C, E, and F are left uninsulated at the bottom of the TES, based on the assumption that lukewarm water accumulates at the TES bottom. Notably, the volume of insulation varies across configurations, with configuration D possessing the largest insulation volume and configuration F the smallest.

Table 4: A summary of the insulation variants considered in this work.

| | $X_{\mathrm{top}}$ [cm] | $X_{\mathrm{side}}$ [cm] | $X_{\mathrm{bot}}$ [cm] | |
|---|---|---|---|---|
| **A** | 53 | 26 | 26 | 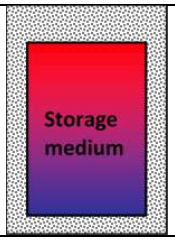  |

| | | | | |
|---|---|---|---|---|
| **B** | 53 | 26 | 0 | 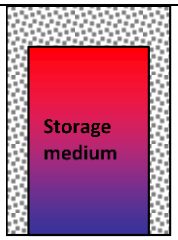 |
| **C** | 53 | 50 %: 26<br>50%: 0 | 0 | 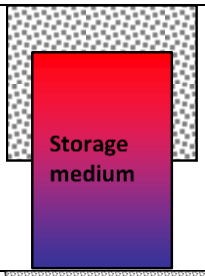 |
| **D** | 53 | *f(r,z)* | 12 | 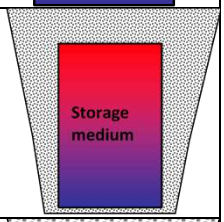 |
| **E** | 53 | *f(r,z)* | 0 | 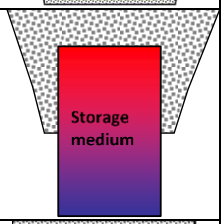 |
| **F** | 53 | 0 | 0 | 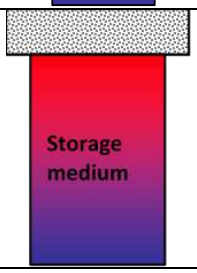 |

Figure 4 illustrates the specific cost for each configuration, showing that configuration D incurs the highest specific cost due to insulation installation on the sidewalls and bottom. Conversely, configuration F exhibits the lowest specific cost as no insulation is applied to the sidewalls or bottom. Compared to D, configuration A has a slightly lower specific cost due to its smaller insulation volume on the sidewalls and bottom. Further, configurations C and E have lower specific costs compared to A, despite only 50% of TES volume being insulated.

These variations in insulation distribution and volume significantly impact TES performance. Fully insulated TES (configuration A) experiences lower thermal losses, allowing more heat to be discharged. However, configuration D emerges as a more promising insulation option, boasting higher performance (e.g., energy efficiency and energy capacity efficiency) by 2.5% compared to configuration A as revealed in Figure 5, attributed to its greater insulation volume. Nonetheless, configuration A exhibits the highest exergy efficiency, indicating superior heat stratification compared to other options (Dahash et al., 2021). In other words, configuration A delivers higher-quality energy for discharged heat. Conversely, configuration D may experience more losses from TES bottom, resulting in colder temperatures and increased mixing, thereby reducing exergy efficiency.

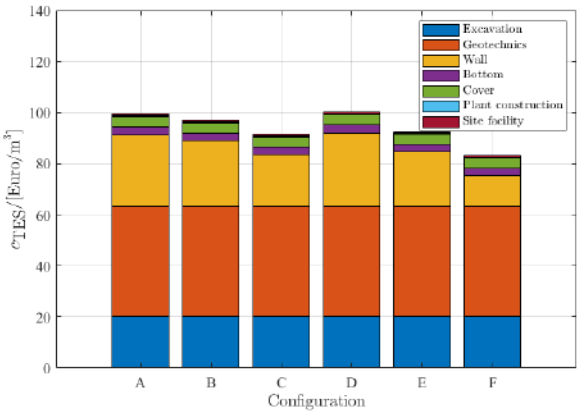


Figure 4: Breakdown of the specific investment cost for a 100,000 m$^3$ fully buried tank installed in HT-DH with several insulation configurations according to the costs reported in Table 3. (Geotechnics cost item refers to diaphragm wall installation, wall cost item refers to insulation cost and liner installations and bottom refers to the installation and cost of insulation and liner).

Figure 6 depicts the LCOS for various tank configurations discussed earlier. Surprisingly, the fully insulated tank exhibits the highest LCOS despite its notable efficiency of 80%. In contrast, the tank in configuration D, featuring gradient insulation, demonstrates a comparatively lower LCOS by 4 €/MWh. Meanwhile, configurations C and E exhibit similar LCOS values. Notably, configurations C and E have only 50% of the buried tank volume insulated in different patterns.

However, this comparison may yield misleading planning decisions due to variations in insulation volume and specific costs across configurations. Thus, the following discussion will compare configurations under two main constraints: 1) maintaining a top insulation thickness of 53 cm and 2) ensuring an insulation volume of 3,616 m$^3$ for all configurations except option F, corresponding to the insulation volume used for configuration D. Additionally, configurations B and E may have greater thickness on the TES sidewalls than on the top due to insulation distribution, necessitating modification. Thus, configurations B and E are assumed to have 80% insulation of the TES volume instead of the previous 50%.

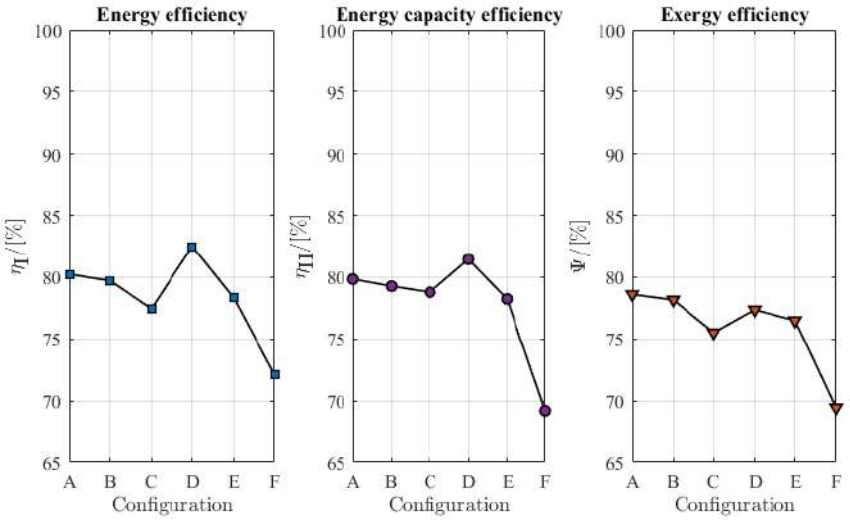


Figure 5: Energetic and exergetic efficiency for the different configurations considered for the insulation distribution for a 100,000 m$^3$ fully buried tank installed in HT-DH.

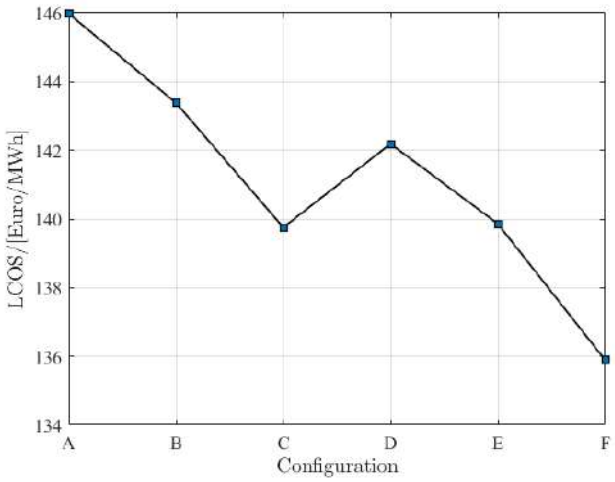


Figure 6: The levelized cost of stored heat for a 100,000 m$^3$ fully buried tank with different insulation configurations reported in Table 4.

Thus, Table 5 reports the adjustments made to configurations to achieve a consistent insulation volume of 3,616 m$^3$. Notably, configuration E represents a buried tank with 80% insulation in a gradient distribution (e.g., truncated cone), with an upper insulation thickness of 53 cm and a lower thickness of 17 cm.

Table 5: A summary of the adjustments for the insulation distribution configuration with an insulation volume of 3,616 m$^3$.

| | $X_{top}$ [cm] | $X_{side}$ [cm] | $X_{bot}$ [cm] |
|---|---|---|---|
| **A** | 53 | 29 | 29 |
| **B** | 53 | 35 | 0 |
| **C** | 53 | 80 %: 26<br>20 %: 0 | 0 |
| **D** | 53 | *f(r,z)* | 12 |
| **E** | 53 | *f(r,z)* | 0 |
| **F** | 53 | 0 | 0 |

Figure 7 presents the breakdown of the specific investment cost for various configurations with a constant insulation volume of 3,616 m$^3$. A minor difference (< 0.5 €/m$^3$) is observed between configurations A, B and D, which slightly increases to 1 €/m$^3$ when considering configurations C and E. Notably, this difference translates to a total of €100,000 for a TES volume of 100,000 m$^3$. While apparently insignificant, this cost disparity could significantly influence decision-making processes, particularly for larger TES volumes exceeding 1,000,000 m$^3$.

Figure 8 displays the energetic and exergetic efficiency for a buried tank with a total insulation volume of 3,616 m$^3$ across different configurations, excluding F. Results indicate the superior performance of D (gradient insulation) compared to its counterparts, demonstrating its ability to recover the highest amount of heat for discharge into the DH. This outcome is attributed to its lower thermal losses, as evidenced by the energy capacity efficiency.

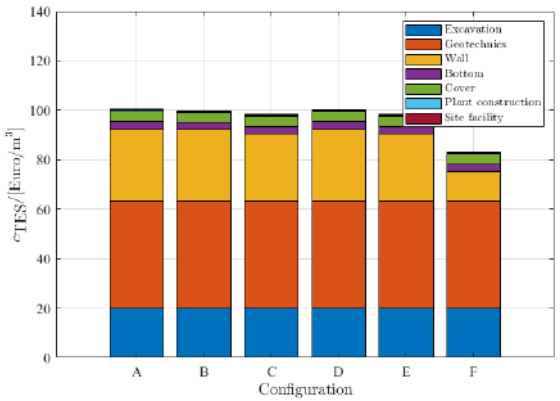


Figure 7: Breakdown of the specific investment cost for a 100,000 m$^3$ fully buried tank installed in HT-DH with several insulation configurations having constant volume of 3616 m$^3$ except configuration F. The costs calculated according to the costs reported in Table 3. (Geotechnics cost item refers to diaphragm wall installation, wall cost item refers to insulation cost and liner installations and bottom refers to the installation and cost of insulation and liner).

Figure 8 reveals another noteworthy finding – the superior performance of B, where TES remains uninsulated at the bottom compared to A, which features full insulation. This highlights the effectiveness of having greater insulation thickness on the sidewalls compared to insulating the bottom under same boundary conditions and constant insulation volume.

Configurations C and E continue to demonstrate comparable performance, consistent with previous findings (compare Figure 5). Additionally, analysis of exergy efficiency reveals superiority of B possessing the highest exergetic efficiency across all configurations – including A and D, where the TES is fully insulated. This result emphasizes the effectiveness of the insulation configuration in configuration B. However, it is important to note that these findings are dependent upon the specified boundary conditions.

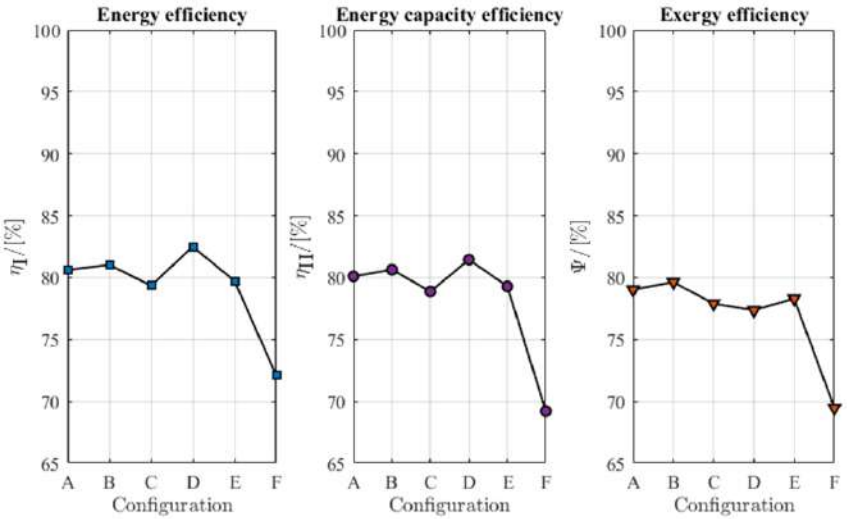


Figure 8: Energetic and exergetic efficiency for the different configurations considered for the insulation distribution for a 100,000 m$^3$ fully buried tank installed in HT-DH.

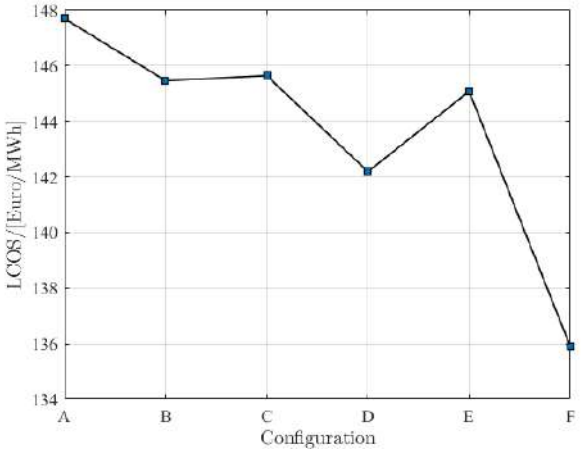


Figure 9: The levelized cost of stored heat for a 100,000 m$^3$ fully buried tank with different insulation configurations with a constant insulation of 3616 m$^3$ except F as reported in Table 5.

Given the high energetic performance of configuration D, Figure 9 shows D yielding the lowest LCOS across the set of insulated TES configurations. Conversely, configurations B and C exhibit comparable LCOS values. Therefore, configuration B may be preferable to C, as it offers higher performance in terms of both energy and exergy.

Despite having a similar specific cost to configurations B and D, moderate performance of configuration A results in the highest LCOS. This emphasizes the importance of proper insulation distribution in the TES envelope to achieve optimal performance and lower LCOS. However, the results also underline the challenge of competing against a non-insulated TES. Insulation may be essential for the TES envelope in environments where groundwater is present as emphasized in (Dahash et al., 2021).

## Conclusions

Large-scale TES offers a great potential to enhance the flexibility and maximize the use of RESs and, thus, TES contributes to the decarbonization. Yet, planning of such large-scale TES systems is challenging due to number of variables that must be iteratively evaluated. One of the critical factors is the insulation level of TES as it has an impact on the techno-economic positioning of large-scale, underground TES.

Via numerical simulations, this work investigated the role of several configurations of insulation in STES pinpointing its critical role in techno-economic feasibility of large-scale TES. The findings suggested that implementing gradient insulation (D) yields optimal energetic performance and moderate LCOS when insulation volume varies. Conversely, maintaining constant insulation volume for insulated options results in the lowest LCOS with optimal energetic performance.

Future research works shall examine the influence of groundwater in the vicinity of STES, exploring prerequisite measures to mitigate its twofold impact. Additionally, our forthcoming work aims to broaden analysis by incorporating an environmental dimension for further explaining the feasibility and sustainability of large-scale TES deployments.

## Acknowledgement

The present study is financially supported by the EU Horizon Europe project INTERSTORES (project no. 101136100). Views and opinions expressed are however those of the author(s) only and do not necessarily reflect those of the European Union or Research Executive Agency.

## References

D'Agostino et al. (2024). Impact of climate change on the energy performance of building envelopes and implications on energy regulations across Europe. *Energy, 288*. doi:10.1016/j.energy.2023.129886.

Dahash et al. (2020). Toward Efficient Numerical Modeling and Analysis of Large-Scale Thermal Energy Storage for Renewable District Heating Systems. *Applied Energy, 279*. doi:DOI: 10.1016/j.apenergy.2020.115840

Dahash et al. (2021). Techno-economic and exergy analysis of tank and pit thermal energy storage for renewables district heating systems. *Renewable Energy, 180*, 1358-1379. doi:10.1016/j.renene.2021.08.106

Dahash et al. (2021). Understanding the interaction between groundwater and large-scale underground hot-water tanks and pits. *Sustainable Cities and Society*. doi:10.1016/j.scs.2021.102928

Huang et al. (2020). Thermal characteristics of a seasonal solar assisted heat pump heating system with an underground tank. *Sustainable Cities and Society, 53*. doi:10.1016/j.scs.2019.101910

Jodeiri et al. (2022). Role of sustainable heat sources in transition towards fourth generation district heating – A review. *Renewable and Sustainable Energy Reviews, 158*. doi:10.1016/j.rser.2022.112156.

K. Johansen and S. Werner. (2022). Something is sustainable in the state of Denmark: A review of the Danish district heating sector. *Renewable and Sustainable Energy Reviews, 158*. doi:10.1016/j.rser.2022.112117.

Maduta et al. (2022). Towards a decarbonised building stock by 2050: The meaning and the role of zero emission buildings (ZEBs) in Europe. *Energy Strategy Reviews, 44*. doi:10.1016/j.esr.2022.101009.

Tosatto et al. (2022). The challenge of planning and constructing large-scale hot water TES for district heating system: A techno-economic analysis. *Proceedings of the International Renewable Energy Storage Conference 2021 (IRES 2021)* (S. 52-66). Atlantis Press. doi:10.2991/ahe.k.220301.006

Yuan et al. (2021). District heating in 100% renewable energy systems: Combining industrial excess heat and heat pumps. *Energy Conversion and Management, 244*. doi:10.1016/j.enconman.2021.114527.